Robust Trajectory Tracking Control for Uncertain 3-DOF Helicopters With Prescribed Performance

Christos K. Verginis, *Member, IEEE*, Charalampos P. Bechlioulis, *Member, IEEE*, Argiris G. Soldatos, and Dimitris Tsipianitis

***Abstract*—This article presents a robust control scheme for the trajectory tracking problem of a three-degree-of-freedom helicopter with prescribed transient and steady-state performance. The control design does not employ any information regarding the dynamics of the system. In addition, the transient and steady-state response of the system with respect to a given time-varying trajectory is *a priori* and explicitly imposed by certain designer-specified performance functions and is fully decoupled from the control gain selection and the dynamic model parameters. Finally, both simulation and experimental results verify the theoretical findings.**

***Index Terms*—Prescribed performance, three-degree-of-freedom (DOF) helicopter, trajectory tracking control.**

I. Introduction

UNMANNED aerial vehicles (UAVs) have drawn considerable attention by researchers during the past few decades owing to their numerous applications, e.g., patrolling, transportation, exploration, search and rescue missions, etc. In particular, unmanned helicopters constitute a compelling class of UAVs, due to their intriguing ability to hover and vertically take-off and land. Typically, such systems are highly nonlinear and underactuated and suffer from severe model uncertainties and dynamic couplings among the various degrees of freedom (DOFs), thus making control design a significantly challenging task. A distinct member of the class of unmanned helicopters that has largely troubled the research community is the three-DOF laboratory helicopter (see Fig. 1). Such a platform emulates the longitudinal motion of actual helicopters and presents significant similarities, in terms of dynamics and underactuation properties, with six-DOF multicopters; hence, it constitutes a prime experimental testbed. At the same time, the three-DOF laboratory helicopter presents unique control challenges due to its underactuation and dynamic couplings, as well as its numerous, potentially uncertain, geometric, and dynamic parameters.

There are a large number of studies in the literature, focusing mainly on the stabilization and trajectory tracking control of three-DOF helicopters. Several works consider linear dynamic models, obtained either by local linearization or feedback linearization techniques [1]–[10]. Nevertheless, local linearization provides a sufficient approximation of the actual dynamics only close to the points/trajectories, with respect to which the linearization is performed. Moreover, linearization techniques usually require *a priori* knowledge of the nonlinear model of the system, which includes dynamic parameters, nonlinearities, and external disturbances that are often difficult to identify. Hence, most of the aforementioned works deal with this issue by assuming uniformly bounded model uncertainties and employing secondary robustifying control terms. In particular, two control frameworks, namely, a quasi-continuous controller and a combination of a sliding-mode observer with a proportional–integral–differential (PID) controller, are presented in [11]. Sliding-mode observers for the bounded uncertainties are also used in [12]; on the other hand, data-driven approaches are used in [3] and [7], a robust H_∞ approach based on gain tuning is pursued in [13], and linear controllers and gain tuning through low-pass filters are used in [9] and [10] to account for the external disturbances. A neural-network-based identification and linearization method is proposed in [6], followed by linear model-predictive control. Input and output constraints are considered in [5], where local linearization around an open-loop trajectory is computed; Iqbal *et al.* [14] take into account input delays and employ discrete algorithms for gain tuning subject to performance metrics. A motion planning approach using virtual holonomic constraints is employed in [8], whereas fuzzy controllers are used in [15]. A computed torque protocol with a disturbance rejection H_∞ controller are combined in [16] and adaptive control techniques are developed in [17]. Furthermore, Shan *et al.* [18] deal with the multiagent synchronization problem and the authors of [4] and [19] perform experimental evaluations, whereas Yang and Zheng [20] employ neural networks for adaptive approximation of the uncertain terms of the model. Finally, Rigatos *et al.* [21]

Manuscript received 12 March 2021; revised 29 July 2021 and 20 October 2021; accepted 28 November 2021. Date of publication 5 January 2022; date of current version 17 October 2022. Recommended by Technical Editor M. Xin and Senior Editor H. Gao. This work was supported by the Research Committee of the University of Patras. *(Corresponding author: Christos K. Verginis.)*

Christos K. Verginis is with the Oden Institute of Computational Engineering and Sciences, University of Texas at Austin, Austin, TX 78705 USA (e-mail: christos.verginis@austin.utexas.edu).

Charalampos P. Bechlioulis and Dimitris Tsipianitis are with the Division of Systems and Control, Department of Electrical and Computer Engineering, University of Patras, 26504 Patras, Greece (e-mail: chmpechl@mail.ntua.gr; dtsipianitis@ece.upatras.gr).

Argiris G. Soldatos is with the Department of Electrical and Computer Engineering, National Technical University of Athens, 15780 Zografou, Greece (e-mail: asoldat@ece.ntua.gr).

Color versions of one or more figures in this article are available at https://doi.org/10.1109/TMECH.2021.3136046.

Digital Object Identifier 10.1109/TMECH.2021.3136046

This work is licensed under a Creative Commons Attribution 4.0 License. For more information, see http://creativecommons.org/licenses/by/4.0/

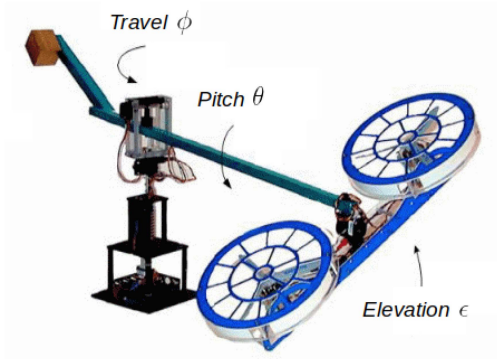

Fig. 1. Quanser three-DOF helicopter.

propose an H_∞ controller based on locally linearized dynamics, and Kocagil *et al.* [22] consider a model reference adaptive control scheme.

Nevertheless, most of the aforementioned works assume either partial or full knowledge of the nominal dynamical model plus a term of uniformly bounded uncertainties, usually compensated via gain tuning. Hence, this considerably restricts the respective control schemes and limits their robustness in realistic scenarios with uncertainties that do not satisfy the aforementioned assumptions. Sliding-mode controllers, robust to dynamic uncertainties, usually employ discontinuous control laws [23] that can cause undesired chattering in real applications. Similarly, standard PID control schemes, which do not explicitly use the model dynamics, cannot provide strong convergence guarantees away from the linearization points. Furthermore, a significant property that lacks from the related literature on three-DOF helicopter control is tracking/stabilization with predefined transient and steady-state specifications, such as overshoot, convergence speed, or steady-state error. Such specifications can encode time and safety constraints, which are crucial when it comes to physical autonomous systems and especially UAVs.

In this article, we develop a modified prescribed performance control (PPC) protocol, which traditionally deals with model uncertainties as well as transient and steady-state constraints [24], to deal with the trajectory tracking control problem for uncertain three-DOF helicopters. The main contributions of this work are as follows:

1) The proposed control protocol does not employ any information on the parameters of the nonlinear dynamic model of the three-DOF helicopter, which renders it significantly robust against model uncertainties and external disturbances.
2) Unlike what is common practice in the related literature, the robustness of the proposed scheme is decoupled from the control gain selection and is independent from the bounds of the nonlinearities of the dynamic model.
3) The tracking errors evolve strictly within a funnel formed by certain designer-specified functions of time that encapsulate performance specifications, thus achieving prescribed transient and steady-state performance.
4) We innovatively adapt the PPC methodology to achieve trajectory tracking with prescribed performance for the elevation and travel angles, since the dynamic model of the three-DOF helicopter is underactuated.

Finally, both comparative simulation results and an experimental study on a real three-DOF helicopter verify the theoretical findings and highlight the aforementioned intriguing attributes. It should be noted that control of three-DOF helicopters with predefined constraints has been considered before in [5], [25], and [26]; however, [25] and [26] do not consider the travel dynamics, rendering the model fully actuated, with the latter also assuming full knowledge of the system's input matrix. Similarly, Kiefer *et al.* [5] consider linear–quadratic regulator control design using local linearization of the dynamics, which are assumed to be known. On the contrary, the present work does not employ any information on the system's dynamic parameters and potential external disturbances.

The rest of this article is organized as follows. Section II provides the necessary notation and preliminary knowledge throughout this article. Section III rigorously formulates the considered problem. The proposed control design is presented in Section IV, while Sections V and VI illustrate its efficiency via simulated and hardware experiments. Finally, Section VII concludes this article.

II. Notation and Preliminaries

A. Dynamical Systems

Theorem 1 (see[27, Ths. 2.1.1(i), 2.1.3]): Let Ω be an open set in $\mathbb{R}^n \times \mathbb{R}_{\geq 0}$. Consider a function $g : \Omega \to \mathbb{R}^n$ that satisfies the following conditions.

1) For every $z \in \mathbb{R}^n$, the function $t \to g(z,t)$ defined on $\Omega_z := \{t : (z,t) \in \Omega\}$ is measurable. For every $t \in \mathbb{R}_{\geq 0}$, the function $z \to g(z,t)$ defined on $\Omega_t := \{z : (z,t) \in \Omega\}$ is continuous.
2) For every compact $S \subset \Omega$, there exist constants C_S, L_S such that $\|g(z,t)\| \leq C_S, \|g(z,t) - g(y,t)\| \leq L_S\|z - y\| \; \forall (z,t),(y,t) \in S$.

Then, the initial value problem

$$\dot{z} = g(z,t), \;\; z_0 = z(t_0) \tag{1}$$

for some $(z_0, t_0) \in \Omega$ has a unique and local solution defined in $[t_0, t_{\max})$, with $t_{\max} > t_0$ such that $(z(t),t) \in \Omega \, \forall t \in [t_0, t_{\max})$.

Theorem 2 (see[27, Th. 2.1.4]): Let the conditions of Theorem 1 hold in Ω and let $t_{\max} > t_0$ be the supremum of all times τ such that the initial value problem (1) has a solution $z(\cdot)$ defined in $[t_0, \tau)$. Then, either $t_{\max} = \infty$ or $\lim_{t \to t_{\max}^-}[\|z(t)\| + \frac{1}{d_S((z(t),t),\partial\Omega)}] = \infty$, where $d_S : \mathbb{R}^n \times 2^{\mathbb{R}^n} \to \mathbb{R}_{\geq 0}$ is the distance of a point $x \in \mathbb{R}^n$ to a set A, defined as $d_S(x,A) := \inf_{y \in A}\{\|x - y\|\}$.

B. Prescribed Performance Control

This subsection presents a summary of preliminary knowledge regarding PPC. The idea of designing controllers that guarantee prescribed transient and steady-state performance specifications was originally introduced in [24]. More specifically, PPC

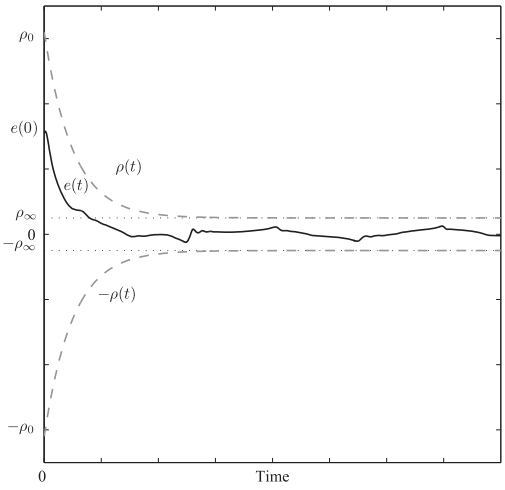

Fig. 2. Graphical illustration of PPC for an exponential performance function $\rho(t)$.

aims at achieving convergence of a scalar tracking error $e(t)$ to a predetermined arbitrarily small residual set with speed of convergence no less than a prespecified value, which is modeled rigorously by $e(t)$ evolving strictly within a predefined region that is upper and lower bounded by certain functions of time, as follows:

$$-\rho(t) < e(t) < \rho(t) \quad \forall t \geq 0 \tag{2}$$

where $\rho(t)$ denotes a smooth and bounded function of time that satisfies $\lim_{t\to\infty} \rho(t) > 0$, called performance function. Fig. 2 illustrates the aforementioned statements for an exponentially decaying performance function, given by

$$\rho(t) := (\rho_0 - \rho_\infty)e^{-\lambda t} + \rho_\infty \tag{3}$$

where ρ_0, ρ_∞, and λ are positive parameters. In particular, the constant ρ_0 is selected such that $\rho_0 > |e(0)|$. Moreover, the parameter $\rho_\infty := \lim_{t\to\infty} \rho(t) > 0$, which represents the maximum allowable value of the steady-state error, can be set to a value reflecting the resolution of the measurement device, so that the error $e(t)$ practically converges to zero. Finally, the constant λ determines the decreasing rate of $\rho(t)$ and, thus, is used to set a lower bound on the convergence rate of $e(t)$. Therefore, the appropriate selection of the performance function $\rho(t)$ imposes certain transient and steady-state performance characteristics on the tracking error $e(t)$.

The key point in PPC is a transformation of the tracking error $e(t)$ that modulates it with respect to the corresponding transient and steady-state performance specifications, encapsulated in the performance function $\rho(t)$. More specifically, we employ a strictly increasing, odd, and bijective mapping $\mathsf{T} : (-1, 1) \to (-\infty, \infty)$. In this article, we adopt the mapping

$$\varepsilon(t) := \mathsf{T}(\xi(t)) := \frac{1}{2} \ln\left(\frac{1+\xi(t)}{1-\xi(t)}\right) \tag{4}$$

that meets the aforementioned properties, with $\xi(t) := \frac{e(t)}{\rho(t)}$ denoting the modulated error. Furthermore, the Jacobian (derivative) of the map $\mathsf{T}(\cdot)$, which is strictly positive by construction, is defined by

$$J_{\mathsf{T}}(\xi) := \frac{\mathrm{d}\mathsf{T}(\xi)}{\mathrm{d}\xi} = \frac{1}{1-\xi^2}. \tag{5}$$

Owing to the properties of the aforementioned transformation, it can be easily verified [28] that preserving the boundedness of $\varepsilon(t)$ is sufficient to achieve prescribed performance, as described in (2).

III. Problem Formulation

Consider a three-DOF laboratory helicopter characterized by its elevation, travel, and pitch angles $\epsilon \in (-\frac{\pi}{2}, \frac{\pi}{2})$, $\phi \in (-\pi, \pi)$, and $\theta \in (-\frac{\pi}{2}, \frac{\pi}{2})$, respectively, with their dynamics described by

$$\ddot{\epsilon} = f_\epsilon(\epsilon, \dot{\epsilon}, t) + a\cos(\theta)V_a \tag{6a}$$

$$\ddot{\phi} = f_\phi(\phi, \dot{\phi}, t) - b\cos(\epsilon)\sin(\theta)V_a \tag{6b}$$

$$\ddot{\theta} = f_\theta(\theta, \dot{\theta}, t) + cV_d \tag{6c}$$

where $f_\epsilon : (-\frac{\pi}{2}, \frac{\pi}{2}) \times \mathbb{R} \times \mathbb{R}_{\geq 0} \to \mathbb{R}$, $f_\phi : (-\pi, \pi) \times \mathbb{R} \times \mathbb{R}_{\geq 0} \to \mathbb{R}$, and $f_\theta : (-\frac{\pi}{2}, \frac{\pi}{2}) \times \mathbb{R} \times \mathbb{R}_{\geq 0} \to \mathbb{R}$ are *unknown* functions that model the gravity, aerodynamics, and external disturbance effects; a, b, and c are *unknown* positive constants; and $V_a := V_f + V_b$ and $V_d := V_f - V_b$ are the common and differential voltage effects, respectively, acting as control inputs, with V_f and V_b denoting the front and back motor voltages. Finally, the functions f_ϵ, f_θ, and f_ϕ are assumed to be continuous in $(\epsilon, \dot{\epsilon})$, $(\theta, \dot{\theta})$, and $(\phi, \dot{\phi})$, respectively, for each $t \in \mathbb{R}_{\geq 0}$, as well as continuous and uniformly bounded in t for each $(\epsilon, \dot{\epsilon})$, $(\theta, \dot{\theta})$, and $(\phi, \dot{\phi})$, respectively. A detailed description of the model (6) may be found in [20].

In this article, we consider the tracking control problem of time-varying reference trajectories $\epsilon_\mathrm{d}(t)$ and $\phi_\mathrm{d}(t)$ for the elevation and travel angles with prescribed performance. PPC, as described in Section II-B, dictates that the tracking error signal evolves strictly within a funnel defined by prescribed functions of time, thus achieving desired performance specifications, such as maximum overshoot, convergence speed, and maximum steady-state error. However, notice that the three-DOF helicopter model (6) is underactuated, and hence, the original PPC methodology cannot be directly applied. Consequently, we innovatively adapt the PPC methodology to achieve trajectory tracking with prescribed performance for the elevation and travel angles ϵ and ϕ.

Before we proceed with the control design, let us consider the bounded reference trajectories $\epsilon_\mathrm{d} : \mathbb{R}_{\geq 0} \to [-\bar{\epsilon}, \bar{\epsilon}] \subset (-\frac{\pi}{2}, \frac{\pi}{2})$ and $\phi_\mathrm{d} : \mathbb{R}_{\geq 0} \to (-\pi, \pi)$, with bounded first and second derivatives, as well as the associated sliding-mode errors:

$$s_\epsilon(\dot{\epsilon}, \epsilon, t) := (\dot{\epsilon} - \dot{\epsilon}_\mathrm{d}(t)) + \lambda_\epsilon(\epsilon - \epsilon_\mathrm{d}(t)) \tag{7a}$$

$$s_\phi(\dot{\phi}, \phi, t) := (\dot{\phi} - \dot{\phi}_\mathrm{d}(t)) + \lambda_\phi(\phi - \phi_\mathrm{d}(t)) \tag{7b}$$

with λ_ϵ and λ_ϕ positive constants. The control objective is to guarantee that the aforementioned error metrics s_ϵ and s_ϕ evolve strictly within a funnel defined by the corresponding exponential performance functions $\rho_\epsilon(t)$ and $\rho_\phi(t)$, which is

rigorously formulated as follows:

$$|s_\epsilon(\dot{\epsilon},\epsilon,t)| < \rho_\epsilon(t) \tag{8a}$$

$$|s_\phi(\dot{\phi},\phi,t)| < \rho_\phi(t) \tag{8b}$$

for all $t \geq 0$, given that initially $|s_\epsilon(\dot{\epsilon}(0),\epsilon(0),0)| < \rho_\epsilon(0)$ and $|s_\phi(\dot{\phi}(0),\phi(0),0)| < \rho_\phi(0)$. The adopted exponentially decaying performance functions are $\rho_\epsilon(t) = (\rho_{\epsilon,0} - \rho_{\epsilon,\infty})\exp(-l_\epsilon t) + \rho_{\epsilon,\infty}$, $\rho_\phi(t) = (\rho_{\phi,0} - \rho_{\phi,\infty})\exp(-l_\phi t) + \rho_{\phi,\infty}$.

Notice that (8) imposes explicit performance specifications on the actual tracking errors $\epsilon - \epsilon_\mathrm{d}$ and $\phi - \phi_\mathrm{d}$ as well. In particular, the first-order linear stable filters (7) with input $s_\epsilon(\dot{\epsilon},\epsilon,t)$ and $s_\phi(\dot{\phi},\phi,t)$ exhibit the following output response:

$$\epsilon(t) - \epsilon_\mathrm{d}(t) = (\epsilon(0) - \epsilon_\mathrm{d}(0))\exp(-\lambda_\epsilon t) + \int_0^t \exp(-\lambda_\epsilon(t-\tau)s_\epsilon(\dot{\epsilon}(\tau),\epsilon(\tau),\tau))d\tau \tag{9a}$$

$$\phi(t) - \phi_\mathrm{d}(t) = (\phi(0) - \phi_\mathrm{d}(0))\exp(-\lambda_\phi t) + \int_0^t \exp(-\lambda_\phi(t-\tau)s_\phi(\dot{\phi}(\tau),\phi(\tau),\tau))d\tau \tag{9b}$$

which, in view of (8), yield

$$|\epsilon(t) - \epsilon_\mathrm{d}(t)| \leq \left(|\epsilon(0) - \epsilon_\mathrm{d}(0)| + \frac{\rho_\epsilon(t)}{\lambda_\epsilon}\right)\exp(-\lambda_\epsilon t) + \frac{\rho_\epsilon(t)}{\lambda_\epsilon} \tag{10a}$$

$$|\phi(t) - \phi_\mathrm{d}(t)| \leq \left(|\phi(0) - \phi_\mathrm{d}(0)| + \frac{\rho_\phi(t)}{\lambda_\phi}\right)\exp(-\lambda_\phi t) + \frac{\rho_\phi(t)}{\lambda_\phi} \tag{10b}$$

which is equivalent to output tracking with prescribed performance, as described in (2). Indeed, by choosing $\lambda_\epsilon > l_\epsilon$, and hence $\exp(-\lambda_\epsilon t) < \exp(-l_\epsilon t)$, we obtain the following equivalent expression:

$$\begin{aligned}|\epsilon(t) - \epsilon_\mathrm{d}(t)| &\leq \left(|\epsilon(0) - \epsilon_\mathrm{d}(0)| + \frac{\rho_\epsilon(t)}{\lambda_\epsilon}\right)\exp(-\lambda_\epsilon t) + \frac{\rho_\epsilon(t)}{\lambda_\epsilon} \\ &\leq \left(|\epsilon(0) - \epsilon_\mathrm{d}(0)| + \frac{\rho_\epsilon(0)}{\lambda_\epsilon}\right)\exp(-l_\epsilon t) + \frac{(\rho_{\epsilon,0} - \rho_{\epsilon,\infty})\exp(-l_\epsilon t)}{\lambda_\epsilon} + \frac{\rho_{\epsilon,\infty}}{\lambda_\epsilon} \\ &\leq \left(|\epsilon(0) - \epsilon_\mathrm{d}(0)| + \frac{2\rho_\epsilon(0)}{\lambda_\epsilon}\right)\exp(-l_\epsilon t) + \frac{\rho_{\epsilon,\infty}}{\lambda_\epsilon}.\end{aligned}$$

An identical relation can be derived for $|\phi(t) - \phi_\mathrm{d}(t)|$ as well.

Remark 1: Except for the guarantees on the convergence rate and the steady-state value of the errors ϵ and ϕ, the proposed framework can also accommodate explicit overshoot specifications. In particular, one could select asymmetric performance functions, i.e., $-\underline{\rho}_\epsilon(t) < s_\epsilon(t) < \bar{\rho}_\epsilon(t)$, $-\underline{\rho}_\phi(t) < s_\phi(t) < \bar{\rho}_\phi(t)$, with one of the two parts appropriately designed to avoid exceeding a desired overshoot level. For more details, we refer the reader to [29].

Remark 2: Although we obtain implicit performance specifications as per (10), the proposed prescribed performance methodology can be extended to account for direct performance specifications on the angle errors $\epsilon - \epsilon_\mathrm{d}$ and $\phi - \phi_\mathrm{d}$, i.e., $|\epsilon(t) - \epsilon_\mathrm{d}(t)| < \rho_\epsilon(t)$, $|\phi(t) - \phi_\mathrm{d}(t)| < \rho_\phi(t)$, by following the backstepping-like methodology of [30].

IV. Main Results

A. Control Design

Let us define the normalized sliding-mode errors

$$\xi_\epsilon(t) := \frac{s_\epsilon(t)}{\rho_\epsilon(t)} \tag{11a}$$

$$\xi_\phi(t) := \frac{s_\phi(t)}{\rho_\phi(t)} \tag{11b}$$

as well as the respective integrals

$$\sigma_\epsilon(t) := \int_0^t \xi_\epsilon(\tau)\,d\tau + \sigma_{\epsilon,0}$$

$$\sigma_\phi(t) := \int_0^t \xi_\phi(\tau)\,d\tau + \sigma_{\phi,0}$$

with $\sigma_{\epsilon,0}$ and $\sigma_{\phi,0}$ appropriately selected constants. We also define the corresponding transformed errors

$$\varepsilon_\epsilon := \mathsf{T}(\xi_\epsilon) \tag{12a}$$

$$\varepsilon_\phi := \mathsf{T}(\xi_\phi) \tag{12b}$$

where $\mathsf{T} : (-1,1) \to (-\infty,\infty)$ is chosen as

$$\mathsf{T}(\mathsf{x}) := \tfrac{1}{2}\ln\left(\tfrac{1+\mathsf{x}}{1-\mathsf{x}}\right). \tag{13}$$

Next, we design: 1) the desired pitch angle command

$$\theta_\mathrm{d} := \arctan\left(-\cos(\epsilon)\frac{J_\mathsf{T}(\xi_\phi)\rho_\epsilon(t)}{J_\mathsf{T}(\xi_\epsilon)\rho_\phi(t)}\frac{(k_{\phi_1}\varepsilon_\phi + k_{\phi_2}\sigma_\phi)}{(k_{\epsilon_1}\varepsilon_\epsilon + k_{\epsilon_2}\sigma_\epsilon)}\right) \tag{14}$$

where $J_\mathsf{T}(\cdot)$ denotes the Jacobian of the transformation $\mathsf{T}(\cdot)$ and k_{ϵ_1}, k_{ϵ_2}, k_{ϕ_1}, and k_{ϕ_2} are positive gains and 2) the common voltage control signal:

$$\begin{aligned}V_a :=\ &\cos(\epsilon)\frac{J_\mathsf{T}(\xi_\phi)}{\rho_\phi(t)}(k_{\phi_1}\varepsilon_\phi + k_{\phi_2}\sigma_\phi)\sin(\theta_\mathrm{d}) \\ &- \frac{J_\mathsf{T}(\xi_\epsilon)}{\rho_\epsilon(t)}(k_{\epsilon_1}\varepsilon_\epsilon + k_{\epsilon_2}\sigma_\epsilon)\cos(\theta_\mathrm{d}).\end{aligned} \tag{15}$$

It should be noted that (14) and (15) lead to

$$\begin{bmatrix}\cos(\theta_\mathrm{d})\,V_a \\ -\sin(\theta_\mathrm{d})\,V_a\end{bmatrix} = \begin{bmatrix}-\frac{J_\mathsf{T}(\xi_\epsilon)\left(k_{\epsilon_1}\varepsilon_\epsilon + k_{\epsilon_2}\sigma_\epsilon\right)}{\rho_\epsilon(t)} \\ -\frac{\cos(\epsilon)J_\mathsf{T}(\xi_\phi)\left(k_{\phi_1}\varepsilon_\phi + k_{\phi_2}\sigma_\phi\right)}{\rho_\phi(t)}\end{bmatrix} \tag{16}$$

which corresponds to the desired force (in magnitude and direction) that should be exerted on the helicopter to achieve trajectory tracking with prescribed performance for the elevation and travel angles. However, the pitch angle does not constitute a control input of the system. Therefore, we define the pitch angle error

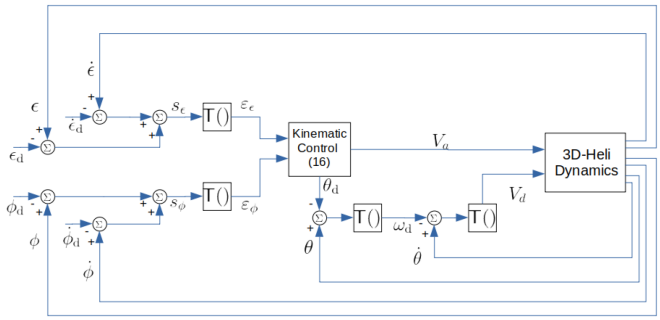

Fig. 3. Block diagram for the proposed PPC control scheme (11)–(20).

$e_\theta = \theta - \theta_\mathrm{d}$ and introduce the corresponding exponential performance function $\rho_\theta(t) := (\rho_{\theta,0} - \rho_{\theta,\infty})\exp(-l_\theta t) + \rho_{\theta,\infty}$, with $\rho_\theta(0) \in (|e_\theta(0)|, \frac{\pi}{2})$. Similarly to (11), we define the normalized pitch angle error

$$\xi_\theta(t) := \frac{e_\theta(t)}{\rho_\theta(t)} \tag{17}$$

and design the desired pitch rate as

$$\omega_\mathrm{d} := -k_\theta \mathsf{T}(\xi_\theta) \tag{18}$$

with $k_\theta > 0$. Following identically the previous step, we define the pitch rate error $e_\omega = \dot\theta - \omega_\mathrm{d}$ and introduce the respective performance function $\rho_\omega(t) := (\rho_{\omega,0} - \rho_{\omega,\infty})\exp(-l_\omega t) + \rho_{\omega,\infty}$, with $\rho_\omega(0) > |e_\omega(0)|$. Finally, we define the normalized pitch rate error as

$$\xi_\omega(t) := \frac{e_\omega(t)}{\rho_\omega(t)} \tag{19}$$

and design the differential voltage control signal as

$$V_d := -k_\omega \mathsf{T}(\xi_\omega) \tag{20}$$

with $k_\omega > 0$. A block diagram illustrating the proposed control scheme is depicted in Fig. 3.

Remark 3: The PPC technique guarantees predefined transient and steady-state performance specifications by enforcing the normalized errors ξ_ϵ, ξ_ϕ, ξ_θ, and ξ_ω to remain strictly within the set $(-1, 1)$ for all $t \geq 0$. Notice that modulating ξ_ϵ, ξ_ϕ, ξ_θ, and ξ_ω via the logarithmic map $\mathsf{T}(\cdot)$, in the control signals (14), (15), (18), and (20), respectively, renders the problem at hand a simple stabilization problem of the modulated errors, as mentioned in Section II-B. Moreover, a careful inspection of the proposed control scheme reveals that it actually operates similarly to reciprocal barrier functions in constrained optimization, admitting high negative or positive values depending on whether $s_\epsilon(t) \to \pm\rho_\epsilon(t)$, $s_\phi(t) \to \pm\rho_\phi(t)$, $e_\theta(t) \to \pm\rho_\theta(t)$, and $s_\omega(t) \to \pm\rho_\omega(t)$; eventually preventing $s_\epsilon(t)$, $s_\phi(t)$, $e_\theta(t)$, and $e_\omega(t)$ from reaching the corresponding boundaries.

B. Stability Analysis

The main results of this article are summarized in the following theorem.

Theorem 3: Consider the three-DOF helicopter dynamics (6) under the control scheme (11)–(20) and assume that

$$|e_\theta(0)| < \frac{\pi}{2} \tag{21a}$$

$$|s_\epsilon(0)| < \frac{\lambda_\epsilon}{2+\lambda_\epsilon}(\bar\pi - \bar\epsilon) \tag{21b}$$

with $\bar\epsilon < \frac{\pi}{2}$ being the upper bound of $|\epsilon_\mathrm{d}(t)|$ and $\bar\pi$ a positive constant satisfying $\bar\pi \in (\bar\epsilon, \frac{\pi}{2})$. Then, selecting the performance functions $\rho_\epsilon(t)$, $\rho_\phi(t)$, $\rho_\theta(t)$, and $\rho_\omega(t)$ such that

$$\rho_\theta(0) \in \left(|e_\theta(0)|, \frac{\pi}{2}\right) \tag{22a}$$

$$\rho_\omega(0) > |e_\omega(0)| \tag{22b}$$

$$\rho_\phi(0) > |s_\phi(0)| \tag{22c}$$

$$\rho_\epsilon(0) > |s_\epsilon(0)| \tag{22d}$$

$$\frac{\rho_\epsilon(0)}{\lambda_\epsilon} < \frac{\bar\pi}{2} - \frac{\bar\epsilon}{2} - \frac{|s_\epsilon(0)|}{2} \tag{22e}$$

the proposed control protocol guarantees that

$$|s_\epsilon(t)| < \rho_\epsilon(t) \tag{23a}$$

$$|s_\phi(t)| < \rho_\phi(t) \tag{23b}$$

for all $t \geq 0$, and consequently that the elevation and travel angles $\epsilon(t)$ and $\phi(t)$ track the desired profiles $\epsilon_\mathrm{d}(t)$ and $\phi_\mathrm{d}(t)$ with prescribed transient and steady-state performance.

Proof: The proof proceeds in the following three steps. We first show, invoking continuity properties, that $\xi_\epsilon(t), \xi_\phi(t), \xi_\theta(t)$, and $\xi_\omega(t)$ remain within $(-1, 1)$ for a time interval $[0, \tau_\mathrm{max})$ (existence of a local solution). Next, we show that the proposed control scheme retains $\xi_\epsilon(t)$, $\xi_\phi(t)$, $\xi_\theta(t)$, and $\xi_\omega(t)$ strictly within compact subsets of $(-1, 1)$, which leads to $\tau_\mathrm{max} = \infty$ (forward completeness) in the final step, thus completing the proof.

Toward the existence of a local solution, first consider the overall state vector $\chi := [\epsilon, \phi, \theta, \sigma_\epsilon, \sigma_\phi, \dot\epsilon, \dot\theta, \dot\phi]^\top \in \mathbb{X}$, where $\mathbb{X} := (-\frac{\pi}{2}, \frac{\pi}{2}) \times (-\pi, \pi) \times (-\frac{\pi}{2}, \frac{\pi}{2}) \times \mathbb{R}^5$ is an open set. Moreover, let us define the open set

$$\Omega := \{(\chi, t) \in \mathbb{X} \times \mathbb{R}_{\geq 0} : \xi_\epsilon \in (1, 1), \xi_\phi \in (-1, 1), \xi_\theta \in (-1, 1), \xi_\omega \in (-1, 1)\} \tag{24}$$

which is nonempty due to (22). Note also that (21b) guarantees that $0 < \frac{|s_\epsilon(0)|}{\lambda_\epsilon} < \frac{\bar\pi}{2} - \frac{\bar\epsilon}{2} - \frac{|s_\epsilon(0)|}{2}$ and, hence, the feasibility of (22d) and (22e). Furthermore, invoking (15) and (20), we obtain the closed-loop system dynamics $\dot\chi = f_\chi(\chi, t)$, where $f_\chi : \mathbb{X} \times \mathbb{R}_{\geq 0} \to \mathbb{R}^8$ is a continuous function in t and locally Lipschitz in χ. Hence, the conditions of Theorem 1 are satisfied, and we conclude that there exists a unique and local solution $\chi : [0, \tau_\mathrm{max}) \to \mathbb{R}^8$, such that $(\chi(t), t) \in \Omega$, for all $t \in [0, \tau_\mathrm{max})$, for a positive $\tau_\mathrm{max} > 0$. Therefore, it holds, for all $t \in [0, \tau_\mathrm{max})$, that

$$\xi_\epsilon(t) \in (-1, 1) \tag{25a}$$

$$\xi_\phi(t) \in (-1, 1) \tag{25b}$$

$$\xi_\theta(t) \in (-1, 1) \tag{25c}$$

$$\xi_\omega(t) \in (-1, 1). \tag{25d}$$

We next proceed to show that the normalized errors in (25) remain in compact subsets of $(-1, 1)$ for all $t \in [0, \tau_\mathrm{max})$.

Note that (25) implies that the transformed elevation and travel errors ε_ϵ and ε_ϕ [see (12)] are well defined for all $t \in [0, \tau_{\max})$. Let us also define $\zeta_\epsilon := \varepsilon_\epsilon + \frac{k_{\epsilon_2}}{k_{\epsilon_1}}\sigma_\epsilon$ and $\zeta_\phi := \varepsilon_\phi + \frac{k_{\phi_2}}{k_{\phi_1}}\sigma_\phi$ and consider the candidate Lyapunov function

$$V := \frac{1}{2}\sigma_\epsilon^2 + \frac{1}{2}\sigma_\phi^2 + \frac{k_{\epsilon_1}}{2a}\zeta_\epsilon^2 + \frac{k_{\phi_1}}{2b}\zeta_\phi^2. \tag{26}$$

Differentiating V along the local solution $\chi(t)$, for all $t \in [0, \tau_{\max})$ yields

$$\dot{V} = \sigma_\epsilon\xi_\epsilon + \sigma_\phi\xi_\phi + \frac{k_{\epsilon_1}}{a}\zeta_\epsilon\left(\frac{J_{\mathsf{T}_\epsilon}}{\rho_\epsilon}(\dot{s}_\epsilon - \dot{\rho}_\epsilon\xi_\epsilon) + \frac{k_{\epsilon_2}}{k_{\epsilon_1}}\xi_\epsilon\right) + \frac{k_{\phi_1}}{b}\zeta_\phi\left(\frac{J_{\mathsf{T}_\phi}}{\rho_\phi}(\dot{s}_\phi - \dot{\rho}_\phi\xi_\phi) + \frac{k_{\phi_2}}{k_{\phi_1}}\xi_\phi\right)$$

where $J_{\mathsf{T}_\epsilon} := J_{\mathsf{T}}(\xi_\epsilon)$ and $J_{\mathsf{T}_\phi} := J_{\mathsf{T}}(\xi_\phi)$. Invoking the inverse logarithmic function from (13) and substituting (6), we obtain

$$\begin{aligned}\dot{V} = {} & \sigma_\epsilon\tanh(\varepsilon_\epsilon) + \sigma_\phi\tanh(\varepsilon_\phi) + k_{\epsilon_1}\zeta_\epsilon\frac{J_{\mathsf{T}_\epsilon}}{\rho_\epsilon}\cos(\theta)V_a \\ & - k_{\phi_1}\zeta_\phi\frac{J_{\mathsf{T}_\phi}}{\rho_\phi}\cos(\epsilon)\sin(\theta)V_a + \frac{k_{\epsilon_2}}{a}\zeta_\epsilon\xi_\epsilon + \frac{k_{\phi_2}}{b}\zeta_\phi\xi_\phi \\ & + \frac{k_{\epsilon_1}}{a}\zeta_\epsilon J_{\mathsf{T}_\epsilon}w_\epsilon(\epsilon,\dot{\epsilon},t) + \frac{k_{\phi_1}}{b}\zeta_\phi J_{\mathsf{T}_\phi}w_\phi(\phi,\dot{\phi},t)\end{aligned} \tag{27}$$

where $w_\epsilon(\epsilon,\dot{\epsilon},t) := \frac{1}{\rho_\epsilon(t)}(f_\epsilon(\epsilon,\dot{\epsilon},t) - \ddot{\epsilon}_{\mathrm{d}}(t) + \lambda_\epsilon(\dot{\epsilon} - \dot{\epsilon}_{\mathrm{d}}(t) - \dot{\rho}_\epsilon(t)\xi_\epsilon))$ and $w_\phi(\phi,\dot{\phi},t) := \frac{1}{\rho_\phi(t)}(f_\phi(\phi,\dot{\phi},t) - \ddot{\phi}_{\mathrm{d}}(t) + \lambda_\phi(\dot{\phi} - \dot{\phi}_{\mathrm{d}}(t) - \dot{\rho}_\phi(t)\xi_\phi))$. For the third and fourth terms in the aforementioned expression, we obtain

$$\begin{aligned}& k_{\epsilon_1}\zeta_\epsilon\frac{J_{\mathsf{T}_\epsilon}}{\rho_\epsilon}\cos(\theta)V_a - k_{\phi_1}\zeta_\phi\frac{J_{\mathsf{T}_\phi}}{\rho_\phi}\cos(\epsilon)\sin(\theta)V_a \\ & = \begin{bmatrix}\zeta_\epsilon & \zeta_\phi\end{bmatrix}\begin{bmatrix}\frac{k_{\epsilon_1}J_{\mathsf{T}_\epsilon}}{\rho_\epsilon} & 0 \\ 0 & \frac{k_{\phi_1}J_{\mathsf{T}_\phi}}{\rho_\phi}\end{bmatrix}\begin{bmatrix}\cos(\theta) \\ -\cos(\epsilon)\sin(\theta)\end{bmatrix}V_a\end{aligned} \tag{28}$$

which, after substituting $\theta = e_\theta + \theta_{\mathrm{d}}$ and expanding the trigonometric identities, becomes

$$\begin{aligned}& k_{\epsilon_1}\zeta_\epsilon\frac{J_{\mathsf{T}_\epsilon}}{\rho_\epsilon}\cos(\theta)V_a - k_{\phi_1}\zeta_\phi\frac{J_{\mathsf{T}_\phi}}{\rho_\phi}\cos(\epsilon)\sin(\theta)V_a = \\ & = \begin{bmatrix}\zeta_\epsilon & \zeta_\phi\end{bmatrix}\begin{bmatrix}\frac{k_{\epsilon_1}J_{\mathsf{T}_\epsilon}}{\rho_\epsilon} & 0 \\ 0 & \cos(\epsilon)\frac{k_{\phi_1}J_{\mathsf{T}_\phi}}{\rho_\phi}\end{bmatrix}R_\theta\begin{bmatrix}\cos(\theta_d) \\ -\sin(\theta_d)\end{bmatrix}V_a\end{aligned}$$

where

$$R_\theta := \begin{bmatrix}\cos(e_\theta) & \sin(e_\theta) \\ -\sin(e_\theta) & \cos(e_\theta)\end{bmatrix}.$$

Finally, by substituting (16) as well as $R_\theta = \frac{R_\theta + R_\theta^\top}{2} + \frac{R_\theta - R_\theta^\top}{2}$, we obtain

$$\begin{aligned}& k_{\epsilon_1}\zeta_\epsilon\frac{J_{\mathsf{T}_\epsilon}}{\rho_\epsilon}\cos(\theta)V_a - k_{\phi_1}\zeta_\phi\frac{J_{\mathsf{T}_\phi}}{\rho_\phi}\cos(\epsilon)\sin(\theta)V_a \\ & = -\cos(e_\theta)k_{\epsilon_1}^2\frac{J_{\mathsf{T}_\epsilon}^2}{\rho_\epsilon^2}\zeta_\epsilon^2 - \cos(e_\theta)\cos(\epsilon)^2k_{\phi_1}^2\frac{J_{\mathsf{T}_\phi}^2}{\rho_\phi^2}\zeta_\phi^2.\end{aligned} \tag{29}$$

From (10) and (25), we obtain $|\epsilon(t)| \leq \bar{\epsilon} + |s_\epsilon(0)| + 2\frac{\rho_\epsilon(0)}{\lambda_\epsilon}$, for $t \in [0, \tau_{\max})$, which, in view of (22e), becomes $|\epsilon(t)| \leq \bar{\pi} < \frac{\pi}{2}$, for $t \in [0, \tau_{\max})$. Therefore, $\cos(\epsilon)^2 \geq \underline{c} := \cos(\bar{\pi})^2 > 0$.

Moreover, by employing the mean value theorem for the terms $\tanh(\varepsilon_\epsilon)$ and $\tanh(\varepsilon_\phi)$, we conclude that there exist $\zeta_{\epsilon_0} \in (\underline{\zeta}_\epsilon, \bar{\zeta}_\epsilon)$ and $\zeta_{\phi_0} \in (\underline{\zeta}_\phi, \bar{\zeta}_\phi)$, where $\underline{\zeta}_\epsilon := \min\{-\frac{k_{\epsilon_2}}{k_{\epsilon_1}}\sigma_\epsilon, -\frac{k_{\epsilon_2}}{k_{\epsilon_1}}\sigma_\epsilon + \zeta_\epsilon\}$, $\underline{\zeta}_\phi := \min\{-\frac{k_{\phi_2}}{k_{\phi_1}}\sigma_\phi, -\frac{k_{\phi_2}}{k_{\phi_1}}\sigma_\phi + \zeta_\phi\}$, and $\bar{\zeta}_\epsilon := \max\{-\frac{k_{\epsilon_2}}{k_{\epsilon_1}}\sigma_\epsilon, -\frac{k_{\epsilon_2}}{k_{\epsilon_1}}\sigma_\epsilon + \zeta_\epsilon\}$, $\bar{\zeta}_\phi := \max\{-\frac{k_{\phi_2}}{k_{\phi_1}}\sigma_\phi, -\frac{k_{\phi_2}}{k_{\phi_1}}\sigma_\phi + \zeta_\phi\}$, such that

$$\left.\frac{d\tanh(\mathsf{x})}{d\mathsf{x}}\right|_{\mathsf{x}=\zeta_{\epsilon_0}} = \frac{\tanh\left(\zeta_\epsilon - \frac{k_{\epsilon_2}}{k_{\epsilon_1}}\sigma_\epsilon\right) + \tanh\left(\frac{k_{\epsilon_2}}{k_{\epsilon_1}}\sigma_\epsilon\right)}{\zeta_\epsilon}$$

$$\left.\frac{d\tanh(\mathsf{x})}{d\mathsf{x}}\right|_{\mathsf{x}=\zeta_{\phi_0}} = \frac{\tanh\left(\zeta_\phi - \frac{k_{\phi_2}}{k_{\phi_1}}\sigma_\phi\right) + \tanh\left(\frac{k_{\phi_2}}{k_{\phi_1}}\sigma_\phi\right)}{\zeta_\phi}$$

which implies that

$$\begin{aligned}\tanh(\varepsilon_\epsilon) = {} & \tanh\left(\zeta_\epsilon - \frac{k_{\epsilon_2}}{k_{\epsilon_1}}\sigma_\epsilon\right) = \zeta_\epsilon(1 - [\tanh(\zeta_{\epsilon_0})]^2) \\ & - \tanh\left(\frac{k_{\epsilon_2}}{k_{\epsilon_1}}\sigma_\epsilon\right)\end{aligned} \tag{30a}$$

$$\begin{aligned}\tanh(\varepsilon_\phi) = {} & \tanh\left(\zeta_\phi - \frac{k_{\phi_2}}{k_{\phi_1}}\sigma_\phi\right) = \zeta_\phi(1 - [\tanh(\zeta_{\phi_0})]^2) \\ & - \tanh\left(\frac{k_{\phi_2}}{k_{\phi_1}}\sigma_\phi\right).\end{aligned} \tag{30b}$$

Substituting (29) and (30) into (27), we obtain

$$\begin{aligned}\dot{V} = {} & -\sigma_\epsilon\tanh\left(\frac{k_{\epsilon_2}}{k_{\epsilon_1}}\sigma_\epsilon\right) - \cos(e_\theta)k_{\epsilon_1}^2\frac{J_{\mathsf{T}_\epsilon}^2}{\rho_\epsilon^2}\zeta_\epsilon^2 \\ & + \frac{k_{\epsilon_2}}{a}\zeta_\epsilon\xi_\epsilon + \frac{1}{a}\zeta_\epsilon J_{\mathsf{T}_\epsilon}w_\epsilon + \zeta_\epsilon\left(1 - [\tanh(\zeta_{\epsilon_0})]^2\right)\end{aligned} \tag{31}$$

$$\begin{aligned}& - \sigma_\phi\tanh\left(\frac{k_{\phi_2}}{k_{\phi_1}}\sigma_\phi\right) - \cos(e_\theta)\underline{c}k_{\phi_1}^2\frac{J_{\mathsf{T}_\phi}^2}{\rho_\phi^2}\zeta_\phi^2 \\ & + \frac{k_{\phi_2}}{b}\zeta_\phi\xi_\phi + \frac{1}{b}\zeta_\phi J_{\mathsf{T}_\phi}^2w_\phi + \zeta_\phi\left(1 - [\tanh(\zeta_{\phi_0})]^2\right).\end{aligned} \tag{32}$$

Moreover, from (9), (10), and (25), one concludes the boundedness of $\epsilon(t)$, $\dot{\epsilon}(t)$, $\phi(t)$, and $\dot{\phi}(t)$ and, hence, the boundedness of the terms $f_\epsilon(\cdot)$ and $f_\phi(\cdot)$, for all $t \in [0, \tau_{\max})$. By invoking the boundedness of ϵ_{d}, ϕ_{d}, and their derivatives, one also concludes the boundedness of $w_\epsilon(\cdot)$ and $w_\phi(\cdot)$ by respective bounds $\bar{\epsilon}$ and $\bar{\phi}$, for all $t \in [0, \tau_{\max})$. In addition, (25) and the fact that $\rho_\theta(t) < \frac{\pi}{2}$ imply that there exists a positive constant $\bar{c}_\theta$ satisfying $\cos(e_\theta(t)) \geq \bar{c}_\theta > 0$, for all $t \in [0, \tau_{\max})$.

Additionally, employing $|\tanh(\cdot)| \leq 1$ and $J_{\mathsf{T}_\epsilon} \geq 1$, $J_{\mathsf{T}_\phi} \geq 1$, $\dot{V}$ becomes

$$\dot{V} \leq -\sigma_\epsilon\tanh\left(\frac{k_{\epsilon_2}}{k_{\epsilon_1}}\sigma_\epsilon\right) - \sigma_\phi\tanh\left(\frac{k_{\phi_2}}{k_{\phi_1}}\sigma_\phi\right) - \bar{c}_\theta k_{\epsilon_1}^2\frac{J_{\mathsf{T}_\epsilon}^2}{\rho_{\epsilon,0}^2}\zeta_\epsilon^2$$

$$-\bar{c}_\theta k_{\phi_1}^2 \frac{J_{\mathsf{T}_\phi}^2}{\rho_{\phi,0}^2}\zeta_\phi^2 + \kappa_\epsilon|\zeta_\epsilon||J_{\mathsf{T}_\epsilon}|\left(\frac{1}{\kappa_\epsilon a}\bar{w}_\epsilon + \frac{k_{\epsilon_2}}{\kappa_\epsilon a} + \frac{1}{\kappa_\epsilon}\right)$$
$$+\kappa_\phi|\zeta_\phi||J_{\mathsf{T}_\phi}|\left(\frac{1}{\kappa_\phi b}\bar{w}_\phi + \frac{k_{\phi_2}}{\kappa_\phi b} + \frac{1}{\kappa_\phi}\right)$$

where κ_ϵ and κ_ϕ are positive constants such that $\mu_\epsilon := \frac{\bar{c}_\theta k_{\epsilon_1}^2}{\rho_{\epsilon,0}^2} - \frac{\kappa_\epsilon}{2} > 0$ and $\mu_\phi := \frac{\bar{c}_\theta k_{\phi_1}^2}{\rho_{\phi,0}^2} - \frac{\kappa_\phi}{2} > 0$. By also denoting $d_\epsilon := (\frac{1}{\kappa_\epsilon a}\bar{w}_\epsilon + \frac{k_{\epsilon_2}}{\kappa_\epsilon a} + \frac{1}{\kappa_\epsilon})$, $d_\phi := (\frac{1}{\kappa_\phi b}\bar{w}_\phi + \frac{k_{\phi_2}}{\kappa_\epsilon b} + \frac{1}{\kappa_\phi})$, $\dot{V}$ finally becomes

$$\dot{V} \leq -\sigma_\epsilon \tanh\left(\frac{k_{\epsilon_2}}{k_{\epsilon_1}}\sigma_\epsilon\right) - \sigma_\phi \tanh\left(\frac{k_{\phi_2}}{k_{\phi_1}}\sigma_\phi\right)$$
$$-\mu_\epsilon\zeta_\epsilon^2 J_{\mathsf{T}_\epsilon}^2 - \mu_\phi\zeta_\phi^2 J_{\mathsf{T}_\phi}^2 + \bar{D}$$

where $\bar{D} := \frac{d_\epsilon^2}{2} + \frac{d_\phi^2}{2}$. Therefore, by invoking [31, Th. 4.18], we conclude that there exist positive and finite constants $\bar{\sigma}_\epsilon$, $\bar{\sigma}_\phi$, $\bar{\varepsilon}_\epsilon$, and $\bar{\varepsilon}_\phi$ such that $|\sigma_\epsilon(t)| \leq \bar{\sigma}_\epsilon$, $|\sigma_\phi(t)| \leq \bar{\sigma}_\phi$, $|\varepsilon_\epsilon(t)| \leq \bar{\varepsilon}_\epsilon$, $|\varepsilon_\phi(t)| \leq \bar{\varepsilon}_\phi$, for all $t \in [0, \tau_{\max})$, which also implies from (12) that

$$|\xi_\epsilon(t)| \leq \bar{\xi}_\epsilon := \tanh(\bar{\varepsilon}_\epsilon) < 1 \tag{33a}$$
$$|\xi_\phi(t)| \leq \bar{\xi}_\phi := \tanh(\bar{\varepsilon}_\phi) < 1 \tag{33b}$$

for all $t \in [0, \tau_{\max})$. Therefore, we conclude the boundedness of θ_{d} and V_a, as designed in (14) and (15), respectively. Based on (25), one also concludes the boundedness of $\theta(t)$ for all $t \in [0, \tau_{\max})$. Differentiating (14) and invoking (33), one may conclude the boundedness of $\dot{\theta}_{\mathrm{d}}$ for all $t \in [0, \tau_{\max})$ as well.

Subsequently, following a similar line of proof, consider the function $V_\theta := \frac{1}{2}\varepsilon_\theta^2$, where $\varepsilon_\theta := \mathsf{T}(\xi_\theta)$. Differentiating and substituting $\dot{\theta} = e_\omega + \omega_{\mathrm{d}}$ and (18), $\dot{V}_\theta$ yields

$$\dot{V}_\theta = -\frac{J_{\mathsf{T}_\theta}}{\rho_\theta}|\varepsilon_\theta|\left(2k_\theta|\varepsilon_\theta| - d_\theta\right) \tag{34}$$

for all $t \in [0, \tau_{\max})$, where $J_{\mathsf{T}_\theta} := J_{\mathsf{T}}(\xi_\theta)$, and d_θ is a positive and finite constant satisfying $d_\theta > |e_\theta(t) - \dot{\theta}_{\mathrm{d}}(t) - \dot{\rho}_\theta(t)\xi_\theta(t)|$, for all $t \in [0, \tau_{\max})$. Hence, we conclude that $\dot{V}_\theta < 0$ when $|\varepsilon| \geq \frac{d_\theta}{k_\theta}$, from which we deduce that there exists a positive and finite constant $\bar{\varepsilon}_\theta$ such that $|\varepsilon_\theta(t)| \leq \bar{\varepsilon}_\theta$ for all $t \in [0, \tau_{\max})$, which further implies that

$$|\xi_\theta(t)| \leq \bar{\xi}_\theta := \tanh(\bar{\varepsilon}_\theta) < 1 \tag{35}$$

and that $\omega_{\mathrm{d}}(t)$ remains bounded, which, in view of (25), also implies the boundedness of $\dot{\theta}(t)$ for all $t \in [0, \tau_{\max})$. Differentiating ω_{d} and invoking (35), one may also conclude the boundedness of $\dot{\omega}_{\mathrm{d}}(t)$ for all $t \in [0, \tau_{\max})$.

Finally, we consider the function $V_\omega := \frac{1}{2}\varepsilon_\omega^2$, with $\varepsilon_\omega := \mathsf{T}(\xi_\omega)$, which, after differentiating and substituting (6) and (20), yields

$$\dot{V}_\omega = -|\varepsilon_\omega|\frac{J_{\mathsf{T}_\omega}}{\rho_\omega}\left(2k_\omega c|\varepsilon_\omega| - d_\omega\right)$$

for all $t \in [0, \tau_{\max})$, where $J_{\mathsf{T}_\omega} := J_{\mathsf{T}}(\xi_\omega)$, and d_ω is a positive and finite constant satisfying $d_\omega > |f_\theta(\theta(t), \dot{\theta}(t), t) - \dot{\omega}_{\mathrm{d}}(t) - \dot{\rho}_\omega(t)\xi_\omega(t)|$, for all $t \in [0, \tau_{\max})$, where we have used the properties of $f_\theta(\cdot)$ to conclude its boundedness from the boundedness of $\theta(t)$ and $\dot{\theta}(t)$. Hence, we conclude that $\dot{V}_\omega < 0$ when $|\varepsilon| \geq \frac{d_\omega}{k_\omega}$, from which we deduce that there exists a positive and finite constant $\bar{\varepsilon}_\omega$ such that $|\varepsilon_\omega(t)| \leq \bar{\varepsilon}_\omega$ for all $t \in [0, \tau_{\max})$, which further implies that

$$|\xi_\omega(t)| \leq \bar{\xi}_\omega := \tanh(\bar{\varepsilon}_\omega) < 1 \tag{36}$$

as well as the boundedness of V_d, as designed in (20), for all $t \in [0, t_{\max})$.

What remains to be shown is that $\tau_{\max} = \infty$. Toward that end, note that (33), (35), and (36) imply that $(\chi(t), t)$ remain in a compact subset of Ω, i.e., there exists a positive constant $\underline{d}$ such that $d_{\mathcal{S}}((\chi(t), t), \partial\Omega) \geq \underline{d} > 0$, for all $[0, \tau_{\max})$. Since all closed-loop signals have been already proved bounded, it holds that $\lim_{t\to\tau_{\max}^-}(\|\chi(t)\| + \frac{1}{d_{\mathcal{S}}((\chi(t),t),\partial\Omega)}) \leq \bar{d}$ for some finite constant $\bar{d}$, and hence, direct application of Theorem 2 dictates that $\tau_{\max} = \infty$, which concludes the proof.

Remark 4: From the aforementioned proof, it can be deduced that the proposed control scheme achieves its goals without resorting to the need of rendering the ultimate bounds $\bar{\varepsilon}_\epsilon$, $\bar{\varepsilon}_\phi$, $\bar{\varepsilon}_\theta$, and $\bar{\varepsilon}_\omega$ of the modulated errors ε_ϵ, ε_ϕ, ε_θ, and ε_ω arbitrarily small by adopting extreme values of the control gains k_{ϵ_1}, k_{ϵ_2}, k_{ϕ_1}, k_{ϕ_2}, k_θ, and k_ω. More specifically, notice that (33), (35), and (36) hold no matter how large the finite bounds $\bar{\varepsilon}_\epsilon$, $\bar{\varepsilon}_\phi$, $\bar{\varepsilon}_\theta$, and $\bar{\varepsilon}_\omega$ are and regardless of the choice of the control gains. In the same spirit, large uncertainties involved in the nonlinear model (6) can be compensated, as they affect only the size of these bounds through $\bar{D}$ and d_ω, but leave unaltered the achieved stability properties. Hence, the actual performance given in (8), which is solely determined by the designer-specified performance functions $\rho_\epsilon(t)$, $\rho_\phi(t)$, $\rho_\theta(t)$, and $\rho_\omega(t)$, becomes isolated against model uncertainties, thus extending greatly the robustness of the proposed control scheme. The only conditions that we impose consist in the initial constraints (21) and (22), which are necessary for the initial compliance with the performance functions as well as the containment of $\epsilon(t)$ in $(-\frac{\pi}{2}, \frac{\pi}{2})$. Given the initial errors $s_\epsilon(0)$, $s_\phi(0)$, $e_\theta(0)$, and $e_\omega(0)$, which can be measured at $t = 0$, one can choose the initial value of the performance functions $\rho_\epsilon(0)$, $\rho_\phi(0)$, $\rho_\theta(0)$, and $\rho_\omega(0)$, respectively, such that (22) hold; note that the feasibility of (22) is guaranteed by (21). Finally, it should be noted that (21b) can be satisfied by appropriately choosing λ_ϵ; substitution of (7) into (21b) yields two second-order algebraic inequalities with respect to λ_ϵ, which lead to new conditions regarding the initial errors $\epsilon(0) - \epsilon_{\mathrm{d}}(0)$, $\dot{\epsilon}(0) - \dot{\epsilon}_{\mathrm{d}}(0)$ as well as design specifications for λ_ϵ. Such conditions, along with (21a), contribute to a conservative estimate of the region of attraction of the closed-loop system. Explicit derivations are beyond the scope of this article and consist part of our future work.

Remark 5: Note that the intermediate control signal $\theta_{\mathrm{d}}(t)$, designed in (14), encounters a singularity when $k_{\epsilon_1}\varepsilon_\epsilon + k_{\epsilon_2}\sigma_\epsilon = k_{\phi_1}\varepsilon_\phi + k_{\phi_2}\sigma_\phi = 0$. However, such singularity can be easily alleviated in practical scenarios by appropriately selecting the performance function ρ_ϵ as well as the initial value of the integrator $\sigma_{\epsilon,0}$. More specifically, notice first that the sign of ε_ϵ coincides with the signs of s_ϵ and ξ_ϵ. Therefore, one could

select asymmetric performance functions (see Remark 1), restricting the evolution of $s_\epsilon(t)$ in a set of the form $(0, \bar{\Gamma})$ if $s_\epsilon(0) \geq 0$ or $(-\bar{\Gamma}, 0)$ if $s_\epsilon(0) < 0$, where $\bar{\Gamma}$ is a positive constant satisfying (22d) and (22e). Hence, by also setting $\sigma_{\epsilon,0}$ such that $\text{sign}(\sigma_{\epsilon,0}) = \text{sign}(s_\epsilon(0))$, we guarantee that $\text{sign}(k_{\epsilon_1}\varepsilon_\epsilon(t) + k_{\epsilon_2}\sigma_\epsilon(t)) = \text{sign}(s_\epsilon(0)) \neq 0$, thus avoiding the aforementioned singularity. Notice also that $s_\epsilon(t)$ still converges to the (arbitrarily small) residual set defined by $\rho_{\epsilon,\infty}$.

Remark 6: It should be noted that the selection of the control gains affects both the quality of evolution of the errors s_ϵ and s_ϕ within the corresponding performance envelopes as well as the control input characteristics. Additionally, fine-tuning might be needed in real-time scenarios, to retain the required control input signals within the feasible range that can be implemented by the actuators. Similarly, the control input constraints impose an upper bound on the required speed of convergence of $\rho_\epsilon(t)$, $\rho_\phi(t)$, as obtained by the exponentials $\exp(-l_\epsilon t)$ and $\exp(-l_\phi t)$, respectively. Hence, the selection of the control gains k_{ϵ_1}, k_{ϵ_2}, k_{ϕ_1}, k_{ϕ_2}, k_θ, and k_ω can have a positive influence on the overall closed-loop system response. More specifically, notice that $\bar{D}$, d_θ, and d_ω provide implicit bounds on $\bar{\varepsilon}_\epsilon$, $\bar{\varepsilon}_\phi$, $\bar{\varepsilon}_\theta$, and $\bar{\varepsilon}_\omega$. Therefore, invoking (14), (15), (18), (20), and (33), we can select the control gains such that V_f and V_b are retained within certain bounds. Nevertheless, the constants $\bar{D}$ and d_ω involve the parameters of the model and the external disturbances. Thus, an upper bound of the dynamic parameters of the system as well as of the exogenous disturbances should be given in order to extract any relations between the achieved performance and the input constraints.

V. Simulation Results

This section is devoted to the validation of the proposed scheme via a comparative simulation study[1] with a recent work [32], which proposes a fault-tolerant scheme based on continuous twisting algorithms (CTA). More specifically, Pérez-Ventura *et al.* [32] consider the set-point regulation problem using linearization around the desired equilibrium and employing appropriately designed observers for the state derivatives. Moreover, the control scheme is shown to be robust to actuator faults of the form of voltage drop. Notice that such faults in both motors can equally be compensated by our control scheme, since the constants a, b, and c in (6) that could be considered strictly positive piecewise constant functions of time (representing uncertain actuator dynamics and faults) are not employed anywhere in the control design, thus leaving unharmed the closed-loop system robustness.

The simulation study consists of two scenarios. First, we considered a nominal case without any external disturbances affecting the dynamics. Subsequently, we considered a perturbed case with sinusoidal disturbances of frequency 0.5 rad/s and amplitude 0.25, 0.2, and 0.1 for the elevation, pitch, and travel dynamics, respectively. Moreover, the values of the parameters that were considered while linearizing the dynamics in [32] deviated up to 10% from their actual simulated values (notice that our method does not employ the parameters of the dynamic model and, therefore, is robust by construction against such type of uncertainties). In both cases, the goal was to drive the system to $(\epsilon, \phi) = (0, 0)$ from the initial condition $(\epsilon(0), \phi(0) = (\frac{\pi}{4}, \frac{\pi}{3})$. For the proposed PPC scheme, we imposed prescribed performance via the exponentially decaying functions $\rho_\epsilon(t) = (|s_\epsilon(0)| + 0.5 - \frac{\pi}{180})\exp(-t) + \frac{\pi}{180}$, $\rho_\phi(t) = (|s_\phi(0)| + 0.5 - \frac{\pi}{180})\exp(-t) + \frac{\pi}{180}$, $\rho_\theta(t) = \frac{44\pi}{90}\exp(-t) + \frac{\pi}{90}$, and $\rho_\omega(t) = (|e_\omega(0)| + 0.5 - \frac{\pi}{90})\exp(-t) + \frac{\pi}{90}$, whereas the control parameters were chosen as $\lambda_\epsilon = \lambda_\phi = 1$, $k_{\epsilon_1} = 2$, $k_{\epsilon_2} = k_{\phi_1} = k_\theta = 2$, $k_\omega = 10$, $k_{\phi_2} = 0.01$, $\sigma_{\epsilon,0} = 0.1$, and $\sigma_{\phi,0} = 0.01$. The control parameters of [32] were chosen as $k_{11} = 5$, $k_{12} = 5$, $k_{13} = 0.1$, $k_{14} = 0$, $k_{21} = 10$, $k_{22} = 10$, $k_{23} = 15$, $k_{24} = 0.3$, $k_{25} = 0$, $k_{26} = 0$, $c = 0.5$, $\lambda_0 = 1.1$, $\lambda_1 = 1.5$, $\lambda_2 = 3$, $\lambda_3 = 5$, and $L = I_3$. Finally, the actuator faults that were simulated corresponded to 25% voltage drop in both motors for all $t \in [5, 10)$ s.

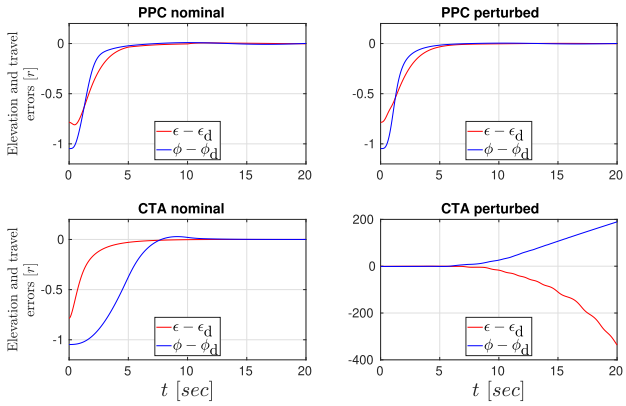

Fig. 4. Evolution of the elevation and travel angle errors. (Top) PPC scheme, in the nominal (left) and perturbed (right) case. (Bottom) CTA scheme, in the nominal (left) and perturbed (right) case.

The results are shown in Fig. 4, where the evolution of the elevation and travel errors $\epsilon(t) - \epsilon_d(t)$ and $\phi(t) - \phi_d(t)$ is depicted during the first 20 s for the proposed PPC and the CTA schemes. In the nominal case, notice that both control schemes establish convergence of the respective errors to zero. In the perturbed case, however, the CTA scheme fails to sustain the stability of the closed-loop system, thus showing large sensitivity in dynamic uncertainties; this can be attributed to the strong reliance of the CTA scheme on the system dynamics. On the other hand, the PPC scheme achieves convergence of the errors to zero even in the perturbed case, verifying the robustness properties exhibited by the theoretical analysis. Furthermore, in order to show the robustness of the proposed PPC scheme, we conducted extra computer simulations for tracking of time-varying reference trajectories using different combinations of the control parameters. The reference elevation and travel trajectories to be tracked were chosen as $\epsilon_d(t) = \frac{15\pi}{180}\sin(\frac{2\pi}{15}t) + \frac{25\pi}{180}$ rad and $\phi_d(t) = \frac{30\pi}{180}\sin(\frac{2\pi}{30}t)$ rad, respectively. The prescribed performance was imposed via the exponentially decaying performance functions $\rho_\epsilon(t) = (1.5 - \frac{\pi}{180})\exp(-t) + \frac{\pi}{180}$, $\rho_\phi(t) = (1.2 - \frac{\pi}{90})\exp(-t) + \frac{\pi}{90}$, $\rho_\theta(t) = \frac{\pi}{2}\exp(-t) + \frac{\pi}{180}$, and $\rho_\omega(t) = (e_\omega(0) + 0.5 - \frac{\pi}{90})\exp(-t) + \frac{\pi}{90}$. Regarding

[1]We adopted the numerical model from [20], including extra additive disturbance terms for the elevation, pitch, and travel dynamics.

TABLE I
SELECTION OF GAINS FOR THE COMPUTER SIMULATIONS

	k_{ϵ_1}	k_{ϵ_2}	k_{ϕ_1}	k_{ϕ_2}	k_θ	k_ω
Case 1	1	1	1	1	1	1
Case 2	3	2	3	2	2	10
Case 3	2	1	2	1	5	20
Case 4	4	4	1	1	2	15
Case 5	1	1	4	4	2	15

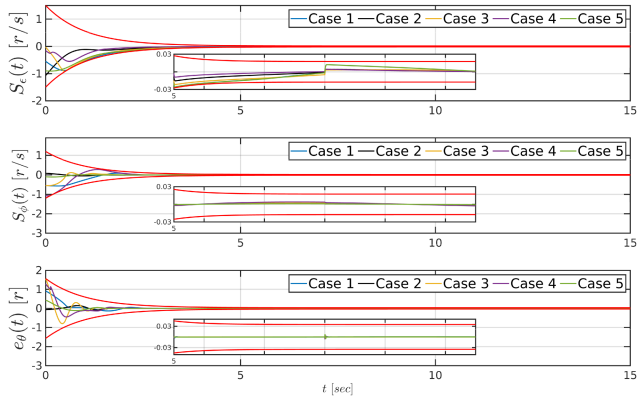

Fig. 5. Evolution of the errors $s_\epsilon(t)$ (top), and $s_\phi(t)$ (middle), and $e_\theta(t)$ (bottom), along with the respective performance functions $\rho_\epsilon(t)$, $\rho_\phi(t)$, and $\rho_\theta(t)$ for the different choices of control gains, according to Table I.

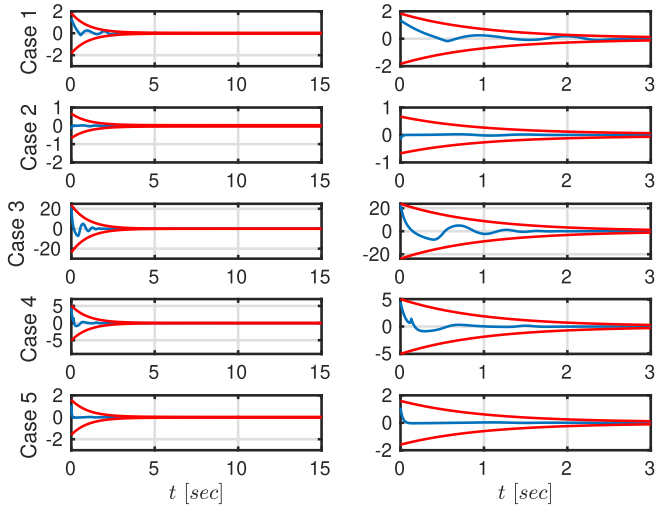

Fig. 6. Evolution of the pitch rate errors $e_\omega(t)$ (in radians per second) along with the respective performance functions $\rho_\omega(t)$ for different choices of control gains, according to Table I. A zoomed-in version is provided in the right part of the figure for $t \in [0, 3]$ s.

the control parameters, we considered the five cases shown in Table I. Finally, for each one of these cases, we chose randomly generated initial conditions for $\epsilon(0)$ and $\phi(0)$ in the interval $(-\frac{\pi}{6}, \frac{\pi}{6})$.

The results are shown in Figs. 5–7 for 15 s. In particular, Fig. 5 illustrates the closed-loop signals $s_\epsilon(t)$, $s_\phi(t)$, and $e_\theta(t)$ along with the respective performance functions $\rho_\epsilon(t)$, $\rho_\phi(t)$, and $\rho_\theta(t)$, and Fig. 6 depicts $e_\omega(t)$ along with the performance functions $\rho_\omega(t)$. Finally, Fig. 7 shows the evolution of the control inputs $V_f(t)$ and $V_b(t)$. It can be concluded from the figures that the errors satisfy the prescribed performance bounds, and all

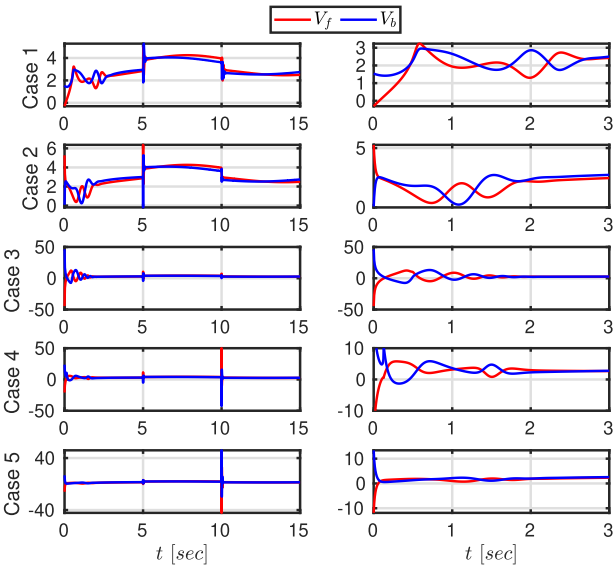

Fig. 7. Evolution of the control inputs $V_f(t)$ and $V_b(t)$ (in volts) for the different choices of control gains, according to Table I. A zoomed-in version is provided in the right part of the figure for $t \in [0, 3]$ s.

closed-loop signals remain bounded, regardless of the control gains' selection. Such a result verifies the theoretical findings, according to which the performance of the closed-loop system is isolated from the unknown terms of the dynamics (6) and the control gain selection; the latter only affect the evolution of the errors in the performance envelopes as well as the magnitude of the resulting control input, as can be verified from the figures. Note also that the proposed control scheme compensates for the imposed actuator faults, resulting in the abrupt changes of the control inputs shown in the right part of Fig. 7 ($t = 5$ and $t = 10$).

VI. EXPERIMENTAL RESULTS

We performed an experimental validation of the proposed methodology on a three-DOF helicopter by Quanser[2] (see Fig. 1). The proposed control algorithm was implemented in Simulink on a PC connected to the helicopter's control unit. The communicated signals consisted of appropriate feedback from the helicopters' onboard sensory system, i.e., the elevation, travel, and pitch angles (the corresponding velocities were calculated numerically by differentiation), as well as the motor voltages V_f and V_b that were calculated by the proposed algorithm as $V_f = \frac{V_a + V_d}{2}$ and $V_b = \frac{V_a - V_d}{2}$ and then were implemented by the power electronics unit.

The reference elevation and travel trajectories to be tracked were chosen as $\epsilon_d(t) = \frac{15\pi}{180}\sin(\frac{2\pi}{15}t) + \frac{25\pi}{180}$ rad and $\phi_d(t) = \frac{30\pi}{180}\sin(\frac{2\pi}{30}t)$ rad, respectively. The prescribed performance was imposed via the exponentially decaying performance functions $\rho_\epsilon(t) = \frac{17\pi}{180}\exp(-0.3t) + \frac{10\pi}{180}$, $\rho_\phi(t) = \frac{35\pi}{18}\exp(-0.2t) + \frac{\pi}{18}$, $\rho_\theta(t) = \frac{4\pi}{9}\exp(-0.5t) + \frac{\pi}{18}$, and $\rho_\omega(t) = \frac{32\pi}{180}\exp(-0.5t) + \frac{15\pi}{180}$. The control parameters were chosen as $\lambda_\epsilon = 2$, $\lambda_\phi = 1$,

[2]Online.: [Available]. https://www.quanser.com/products/3-dof-helicopter/

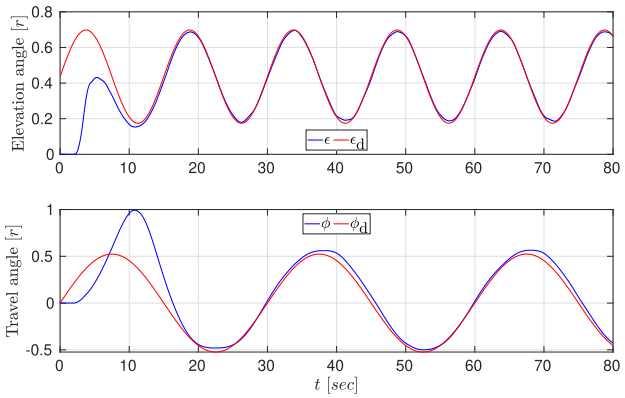

Fig. 8. Evolution of the elevation signals $\epsilon(t)$ and $\epsilon_{\mathrm{d}}(t)$ (top) and travel signals $\phi(t)$ and $\phi_{\mathrm{d}}(t)$ (bottom).

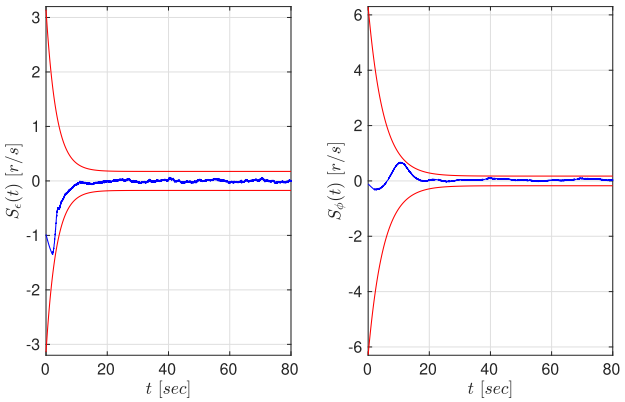

Fig. 9. Evolution of the sliding surface errors $s_\epsilon(t)$ (left) and $s_\phi(t)$ (right), depicted with blue, along with the corresponding performance functions $\rho_\epsilon(t)$ and $\rho_\phi(t)$, depicted with red.

$k_{\epsilon_1} = 0.75$, $k_{\epsilon_2} = 0.5$, $k_{\phi_1} = 0.5$, $k_{\phi_2} = 0.01$, $k_\theta = k_\omega = 1$, $\sigma_{\epsilon,0} = -0.1$, and $\sigma_{\phi,0} = 0$. Finally, the initial pose and velocity of the helicopter was $\epsilon(0) = \dot{\epsilon}(0) = \theta(0) = \dot{\theta}(0) = \phi(0) = \dot{\phi}(0) = 0$, creating the initial conditions $s_\epsilon(0) = -0.983$, $s_\phi(0) = -0.219$, $e_\theta(0) = 0.046$, and $e_\omega(0) = 0.0586$. We stress that, since the problem studied in this article is tracking of a time-varying trajectory, the values of the initial errors do not affect the performance of the closed-loop system, since the dynamics of the trajectory to be tracked tend to disturb it from its initial position.

The results are depicted in Figs. 8–11 during the first 80 s of the experiment. In particular, Fig. 8 shows the evolution of the elevation and travel angles $\epsilon(t)$ and $\phi(t)$ along with the reference signals $\epsilon_{\mathrm{d}}(t)$ and $\phi_{\mathrm{d}}(t)$. Moreover, Fig. 9 shows the evolution of the sliding surface errors $s_\epsilon(t)$ and $s_\phi(t)$ along with the corresponding performance functions $\rho_\epsilon(t)$ and $\rho_\phi(t)$. Similarly, Fig. 10 illustrates the evolution of the pitch angle and rate errors $e_\theta(t)$ and $e_\omega(t)$, along with the respective performance functions $\rho_\theta(t)$, $\rho_\omega(t)$. Finally, Fig. 11 depicts the required motor voltages $V_f(t)$ and $V_b(t)$. The observed chattering can be attributed to sensor imperfections, the discrete implementation of the control algorithm, and the small final values of the performance functions $(\rho_{\epsilon,\infty}, \rho_{\phi,\infty}, \rho_{\theta,\infty}, \rho_{\omega,\infty})$. It is apparent, nevertheless, that the chattering corresponds to less than 10% of the magnitude of the depicted signals and does

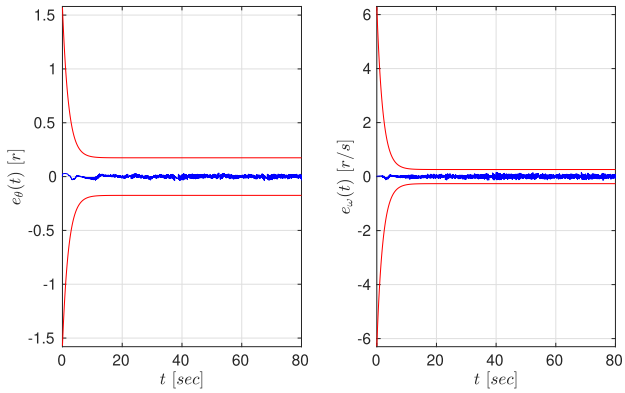

Fig. 10. Evolution of the pitch angle and rate errors $e_\theta(t)$ (left) and $e_\omega(t)$ (right), depicted with blue, along with the corresponding performance functions $\rho_\theta(t)$ and $\rho_\omega(t)$, depicted with red.

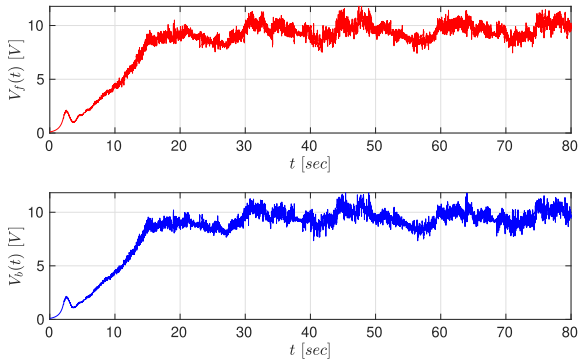

Fig. 11. Required motor voltages $V_f(t)$ (top) and $V_b(t)$ (bottom).

not affect the performance of the closed-loop system; the desired trajectory is accurately tracked while satisfying the prescribed performance specifications and exhibiting easily implementable voltage signals, thus validating the theoretical findings. A short video illustrating the aforementioned experiment can be found at https://youtu.be/jBdOW-C-eYs.

VII. Conclusion

In this article, we proposed a robust control protocol for the trajectory tracking of a three-DOF helicopter by using the prescribed performance methodology. Certain user-defined functions dictate the transient and steady-state response of the system. The proposed methodology was validated using extensive simulation and experimental results. Future efforts will be devoted toward extending the presented framework to more general classes of underactuated vehicles as well as considering multiagent scenarios.

References

[1] M. Lopez-Martinez, J. Diaz, M. Ortega, and F. Rubio, "Control of a laboratory helicopter using switched 2-step feedback linearization," in *Proc. Amer. Control Conf.*, 2004, vol. 5, pp. 4330–4335.

[2] H. Liu, G. Lu, and Y. Zhong, "Robust output tracking control of a laboratory helicopter for automatic landing," *Int. J. Syst. Sci.*, vol. 45, no. 11, pp. 2242–2250, 2014.

[3] W. Gao and Z.-P. Jiang, "Data-driven adaptive optimal output-feedback control of a 2-DOF helicopter," in *Proc. Amer. Control Conf.*, 2016, pp. 2512–2517.

[4] A. Prach, E. Kayacan, and D. S. Bernstein, "An experimental evaluation of the forward propagating Riccati equation to nonlinear control of the Quanser 3 DOF Hover testbed," in *Proc. Amer. Control Conf.*, 2016, pp. 3710–3715.
[5] T. Kiefer, K. Graichen, and A. Kugi, "Trajectory tracking of a 3DOF laboratory helicopter under input and state constraints," *IEEE Trans. Control Syst. Technol.*, vol. 18, no. 4, pp. 944–952, Jul. 2010.
[6] J. Witt, S. Boonto, and H. Werner, "Approximate model predictive control of a 3-DOF helicopter," in *Proc. 46th IEEE Conf. Decis. Control*, 2007, pp. 4501–4506.
[7] W. Gao, M. Huang, Z.-P. Jiang, and T. Chai, "Sampled-data-based adaptive optimal output-feedback control of a 2-degree-of-freedom helicopter," *IET Control Theory Appl.*, vol. 10, no. 12, pp. 1440–1447, 2016.
[8] I. M. Meza-Sánchez, L. T. Aguilar, A. Shiriaev, L. Freidovich, and Y. Orlov, "Periodic motion planning and nonlinear H^∞ tracking control of a 3-DOF underactuated helicopter," *Int. J. Syst. Sci.*, vol. 42, no. 5, pp. 829–838, 2011.
[9] B. Zheng and Y. Zhong, "Robust attitude regulation of a 3-DOF helicopter benchmark: Theory and experiments," *IEEE Trans. Ind. Electron.*, vol. 58, no. 2, pp. 660–670, Feb. 2011.
[10] H. Liu, G. Lu, and Y. Zhong, "Robust LQR attitude control of a 3-DOF laboratory helicopter for aggressive maneuvers," *IEEE Trans. Ind. Electron.*, vol. 60, no. 10, pp. 4627–4636, Oct. 2013.
[11] H. RÍos, A. Rosales, A. Ferreira, and A. Dávilay, "Robust regulation for a 3-DOF helicopter via sliding-modes control and observation techniques," in *Proc. Amer. Control Conf.*, 2010, pp. 4427–4432.
[12] A. F. De Loza, H. RÍos, and A. Rosales, "Robust regulation for a 3-DOF helicopter via sliding-mode observation and identification," *J. Franklin Inst.*, vol. 349, no. 2, pp. 700–718, 2012.
[13] X. Wang, G. Lu, and Y. Zhong, "Robust H^∞ attitude control of a laboratory helicopter," *Robot. Auton. Syst.*, vol. 61, no. 12, pp. 1247–1257, 2013.
[14] A. Iqbal, O. Roesch, H. Roth, and A. Rasool, "Using meta-heuristics in the control of a non-linear input delay laboratory helicopter system," in *Proc. 44th IEEE Conf. Decis. Control*, 2005, pp. 4047–4052.
[15] K. Tanaka, H. Ohtake, and H. O. Wang, "A practical design approach to stabilization of a 3-DOF RC helicopter," *IEEE Trans. Control Syst. Technol.*, vol. 12, no. 2, pp. 315–325, Mar. 2004.
[16] M. Lopez-Martinez, C. Vivas, and M. Ortega, "A multivariable nonlinear H^∞ controller for a laboratory helicopter," in *Proc. 44th IEEE Conf. Decis. Control*, 2005, pp. 4065–4070.
[17] B. Andrievsky, D. Peaucelle, and A. L. Fradkov, "Adaptive control of 3DOF motion for LAAS helicopter benchmark: Design and experiments," in *Proc. Amer. Control Conf.*, 2007, pp. 3312–3317.
[18] J. Shan, H.-T. Liu, and S. Nowotny, "Synchronised trajectory-tracking control of multiple 3-DOF experimental helicopters," *Proc. Inst. Elect. Eng.—Control Theory Appl.*, vol. 152, no. 6, pp. 683–692, 2005.
[19] A. T. Kutay, A. J. Calise, M. Idan, and N. Hovakimyan, "Experimental results on adaptive output feedback control using a laboratory model helicopter," *IEEE Trans. Control Syst. Technol.*, vol. 13, no. 2, pp. 196–202, Mar. 2005.
[20] X. Yang and X. Zheng, "Adaptive NN backstepping control design for a 3-DOF helicopter: Theory and experiments," *IEEE Trans. Ind. Electron.*, vol. 67, no. 5, pp. 3967–3979, May 2020.
[21] G. Rigatos, P. Wira, M. Hamida, M. Abbaszadeh, and J. Pomares, "Nonlinear optimal control for the 3-DOF laboratory helicopter," in *Proc. IEEE 29th Int. Symp. Ind. Electron.*, 2020, pp. 555–560.
[22] B. M. Kocagil, S. Ozcan, A. C. Arican, U. M. Guzey, E. H. Copur, and M. U. Salamci, "MRAC of a 3-DOF helicopter with nonlinear reference model," in *Proc. 26th Mediterranean Conf. Control Autom.*, 2018, pp. 1–6.
[23] Y. Orlov, M. Meza-Sánchez, and L. T. Aguilar, "Sliding mode velocity-observer-based stabilization of a 3-DOF helicopter prototype," *IFAC Proc. Vol.*, vol. 42, no. 6, pp. 179–184, 2009.
[24] C. P. Bechlioulis and G. A. Rovithakis, "Robust adaptive control of feedback linearizable MIMO nonlinear systems with prescribed performance," *IEEE Trans. Autom. Control*, vol. 53, no. 9, pp. 2090–2099, Oct. 2008.
[25] H. Yang, B. Jiang, H. Yang, and H. H. Liu, "Synchronization of multiple 3-DOF helicopters under actuator faults and saturations with prescribed performance," *ISA Trans.*, vol. 75, pp. 118–126, 2018.
[26] X. Wang, "Smooth attitude tracking control of a 3-DOF helicopter with guaranteed performance," 2021, *arXiv:2101.11241*.
[27] A. Bressan and B. Piccoli, *Introduction to the Mathematical Theory of Control*, vol. 2. Springfield, MO, USA: Amer. Inst. Math. Sci, 2007.
[28] C. P. Bechlioulis and G. A. Rovithakis, "Prescribed performance adaptive control for multi-input multi-output affine in the control nonlinear systems," *IEEE Trans. Autom. Control*, vol. 55, no. 5, pp. 1220–1226, May 2010.
[29] A. Theodorakopoulos and G. A. Rovithakis, "Low-complexity prescribed performance control of uncertain MIMO feedback linearizable systems," *IEEE Trans. Autom. Control*, vol. 61, no. 7, pp. 1946–1952, Jul. 2016.
[30] C. P. Bechlioulis and G. A. Rovithakis, "A low-complexity global approximation-free control scheme with prescribed performance for unknown pure feedback systems," *Automatica*, vol. 50, no. 4, pp. 1217–1226, 2014.
[31] H. K. Khalil, *Nonlinear Systems*. Englewood Cliffs, NJ, USA: Prentice-Hall, 2002.
[32] U. Pérez-Ventura, L. Fridman, E. Capello, and E. Punta, "Fault tolerant control based on continuous twisting algorithms of a 3-DOF helicopter prototype," *Control Eng. Pract.*, vol. 101, 2020, Art. no. 104486.

Christos K. Verginis (Member, IEEE) was born in Athens, Greece, in 1989. He received the Diploma degree in electrical and computer engineering and the M.Sc. degree in automatic control systems and robotics from the National Technical University of Athens, Zografou, Greece, in 2013 and 2015, respectively, and the Ph.D. degree in electrical engineering from the KTH Royal Institute of Technology, Stockholm, Sweden, in 2020.

He is currently a Postdoctoral Researcher with the Oden Institute for Computational Engineering and Sciences, University of Texas at Austin, Austin, TX, USA. He has authored more than 30 papers in scientific journals and conference proceedings. His research interests include nonlinear and adaptive control, hybrid and safety-critical systems, multirobot systems, data-driven control, and reinforcement learning.

Charalampos P. Bechlioulis (Member, IEEE) was born in Arta, Greece, in 1983. He received the Diploma degree in electrical and computer engineering (Hons.), the Bachelor of Science degree in mathematics (second in his class), and the Ph.D. degree in electrical and computer engineering from the Aristotle University of Thessaloniki, Thessaloniki, Greece, in 2006, 2011, and 2011, respectively.

He is currently an Associate Professor with the Department of Electrical and Computer Engineering, University of Patras, Patras, Greece. He has authored more than 90 papers in scientific journals and conference proceedings and three book chapters. His research interests include nonlinear control with prescribed performance, system identification, control of robotic vehicles, and multiagent systems.

Argiris G. Soldatos received the Bachelor of Science in mathematics and engineering from University of Manchester, Institute of Science and Technology, in 1985, and Bachelor of Science in mathematics and engineering from University of California at Berkeley, in 1988.

He is currently with the Department of Electrical and Computer Engineering, National Technical University of Athens, Zografou, Greece. His current research interests include dynamical systems and control.

Dimitris Tsipianitis received the Diploma degree in electrical and computer engineering from the University of Patras, Patras, Greece, in 1997, and the M.Sc. degree in adults education from Hellenic Open University, Thermi, Greece, in 2015.

He was born in Patras, Greece, in 1973. Since 2003, he has been a Laboratory Lecturer with the Laboratory for Automation and Robotics, Department of Electrical and Computer Engineering, University of Patras, Patras. He was a Researcher and a Project Manager in international projects as well as with the Intel Company and the Atmel Company as a Hardware Engineer and a Project Manager. His research interests include electrical circuits and printed circuit board design technologies, robotic systems, digital control, information technology, and distance learning technics and evaluation.